Time-Dependent Three-Dimensional Intravascular Ultrasound

Jed Lengyel* Cornell University
Donald P. Greenberg† Cornell University
Richard Popp‡ Stanford University

Abstract

Intravascular ultrasonography and x-ray angiography provide two complimentary techniques for imaging the moving coronary arteries. We present a technique that combines the strengths of both, by recovering the moving three-dimensional arterial tree from a stereo pair of angiograms through the use of compound-energy "snakes", placing the intravascular ultrasound slices at their proper positions in time and space, and dynamically displaying the combined data.

Past techniques have assumed that the ultrasound slices are parallel and that the vessel being imaged is straight.

For the first time, by applying simple but effective techniques from computer graphics, the *moving* geometry of the artery from the angiogram and the *time-dependent* images of the interior of the vessel wall from the intravascular ultrasound can be viewed simultaneously, showing the proper geometric and temporal relations of the slice data and the angiogram projections. By using texture-mapped rectangles the combined ultrasound slice/angiogram display technique is well suited to run in real time on current graphics workstations.

CR Categories and Subject Descriptors: I.3.0 [Computer Graphics]: General; I.3.8 [Computer Graphics]: Applications. J.3 [Life and Medical Sciences].

1 Introduction

Although the current trend in medical imaging is towards non-invasive and low-radiation techniques such as MRI (magnetic resonance imaging), for cardiac patients there is still a need for high-resolution, high-detail information particularly for planning coronary treatments such as bypass surgery, balloon angioplasty, and atherectomy. No current non-invasive imaging technique can provide the accurate high-resolution data required for these decisions at the present time.

Intravascular ultrasound imaging is a relatively new technique for imaging the interior structure of arteries and provides one method for obtaining such high-detail images.[14][15] Unlike traditional cardiac ultrasound that uses an exterior probe and is limited to imaging between the patient's ribs or a transesophageal probe, intravascular ultrasound uses a miniature ultrasound transducer mounted on the tip of a catheter. (Figure 1(a))

To image the coronary arteries, both intravascular ultrasound and standard contrast angiograms use the same catheter placement technique. The catheter is threaded inside the patient's arterial system through an artery in the thigh, and then maneuvered through the descending aorta, around the aortic arch, and into the coronary arteries. For contrast angiograms, radio-opaque dye is injected at the catheter's tip so that the blood flow in the lumen of the vessel appears in fluoroscopic x-ray images. For intravascular ultrasound, the transducer at the tip of the catheter is rotated by a drive shaft that runs the length of the catheter. The rotating transducer can then image cross-sections by emitting pulses of ultrasound (currently in the 20-50 MHz range) and then receiving time-delayed echos. (Figure 1(b))

The main advantage of intravascular ultrasound over the standard contrast angiogram is that intravascular ultrasound can make images of the interior structure of the artery wall. Although the resolution of ultrasound devices is generally lower than other imaging methods, because of the small field of view and lack of any obstructing tissue, and the reduction of noise with intravascular positioning, fine detail structure can be obtained. The standard angiogram shows only a two-dimensional projection of the lumen of the vessel. (Figure 1(c) and Figure 1(d)) Recently it has been shown that intravascular ultrasound can both reveal disease that does not appear in the standard constrast angiogram and accurately measure the vessel lumen.[10][9] (Figure 1(e) and Figure 1(f))

Previous work on three-dimensional reconstruction of two-dimensional ultrasound slices has been limited to static geometries and has assumed that the vessel being imaged was straight. Visualizations were composed of stacked slices to form three dimensional cylindrical images. [8] [4] [2] The images produced in this way show the three-dimensional relations of vessel structures, but distort the geometry.[7] Furthermore, slices collected from different times in the heart cycle are shown together. Previous research by the authors has extended these procedures to handle a static but curved arterial tree.[5]

This paper describes a prototypical system which uses advanced computer graphics techniques to:

- Accurately reconstruct the three-dimensional geometry of the coronary arterial tree from two-dimensional angiograms through the use of compound-energy "snakes."
- Precisely position time-dependent, two-dimensional ultrasound slices on the dynamic arterial tree.
- Dynamically display the combined data for medical diagnosis.

The interactive system can run on an advanced graphics workstation and provide immediate feedback to the cardiac surgeon/cardiologist.

* *Current address:* One Microsoft Way, Redmond WA 98052-6399, jedl@microsoft.com.
† 580 ETC, Ithaca, NY 14850. dpg@graphics.cornell.edu.
‡ School of Medicine, Stanford, CA 94305.

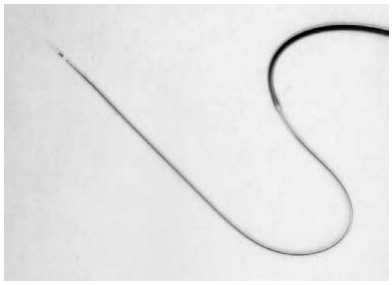

(a) Catheter for Intravascular Imaging

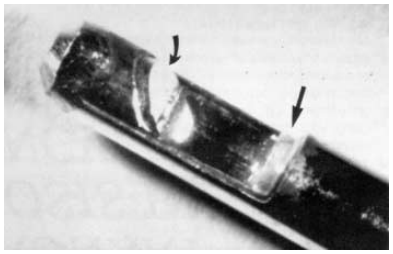

(b) Detail of Transducer

(c) Standard Angiogram — Left Anterior Oblique

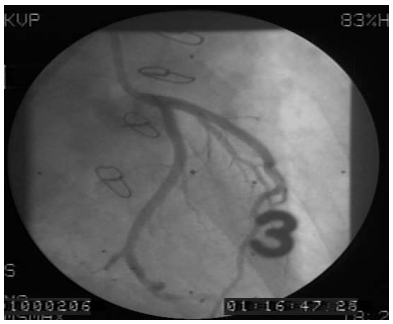

(d) Standard Angiogram — Right Anterior Oblique

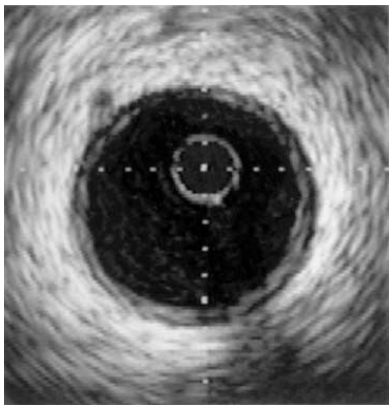

(e) Typical Intravascular Ultrasound Cross-Section of a Normal Adult Coronary Atery

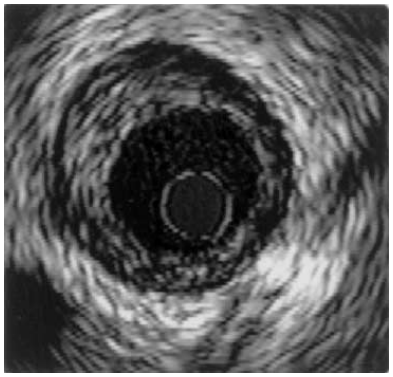

(f) Cross-Section of a Diseased Coronary Artery — The eccentric plaque (soft gray echoes) surrounds the blood-filled vessel lumen (black).

Figure 1: Data Input Devices and Examples

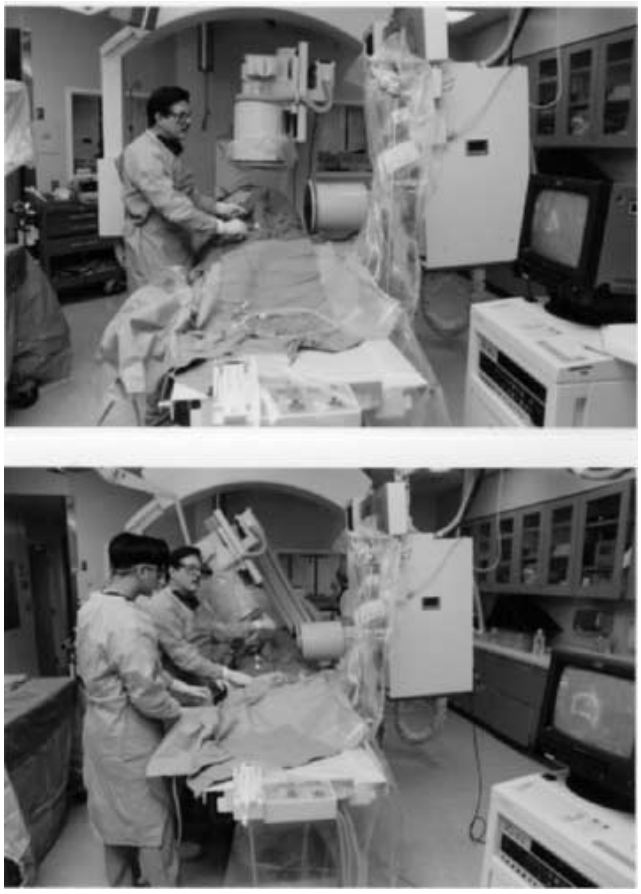

Figure 2: Hospital with patient being imaged by a biplane angiogram.

2 Geometry of the Arterial Centerline

Determining the centerline of a dynamic three-dimensional arterial tree is non-trivial. Standard angiograms have poor contrast, poor signal to noise ratios, and, most importantly, changing points of discontinuity caused by the overlapping projections of the branches of the arterial tree. Standard edge-tracking methods easily get confused, requiring frequent user intervention.

Our initial technique for reconstructing a segment of the arterial tree was an interactive one in which the stereo angiograms were presented to the user who then positioned points along the length of the artery segment in both images. Standard stereo inverse techniques were then used to calculate the three-dimensional points.[6] This technique was far too labor intensive to be useful, especially when considering the goal of capturing the *moving* geometry of the arterial tree. The goal of automatic tracking motivated the use of the technique described below.

Since arteries are made of elastic material, the model we use to fit to the arteries should capture this behavior. One such model used in computer vision is energy-based splines, or "snakes". Snakes have been used to track edges, to follow moving features, and to perform stereo matching—all of which are needed for tracking a moving artery. [3][1] Our work differs from the previous work by the use of compound snakes with offset energy functions. The use of a centerline and symmetric offsets is similar to the more general three-dimensional symmetry-seeking models found in [11].

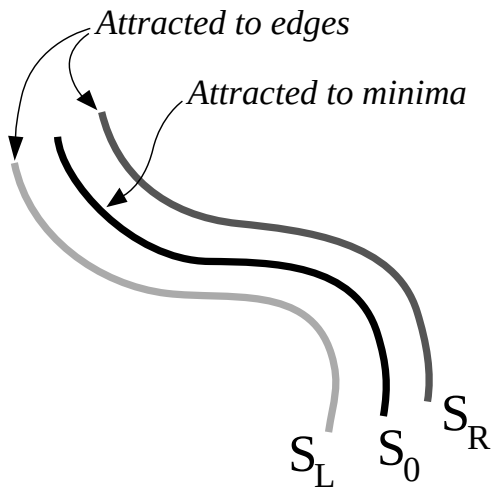

Figure 3: Snake — Physically-based spline attracted to image features specified in energy functions.

2.1 Energy-Minimizing Splines

Snakes are modeled with an internal elastic energy, E_{internal}, and external energy functions, E_{external}. The internal energy gives the snake its elastic character. The external energy functions are important for getting a desired behavior. For example, if one uses an energy such as $E_{\text{external}}(x,y) = I(x,y)$ where I is the image intensity, by minimizing the energy function, the snake will seek dark areas in the image.

To make a good artery tracker, we use a combination snake with a center and two offset sides and the following energies (Figure 3):

- Minima-seeking, $E_{\text{minima}} = I(x,y)$
- Edge-tracking, $E_{\text{edge}} = -|\nabla I(x,y)|^2$

Let $s_C(u)$ be the centerline of the snake. We will define $s_L(u)$ and $s_R(u)$ to be perpendicularly offset from $s_C(u)$ at each u by r_{width}. Let

$$\begin{aligned} s_L(u) &= s_C(u) + r_{\text{width}} n(u) \\ s_R(u) &= s_C(u) - r_{\text{width}} n(u) \end{aligned}$$

where $n(u)$ is the normal to the curve of $s_C(u)$. Using these curves, we can define the following energy to minimize:

$$\begin{aligned} E_{\text{external}}(u) = {} & k_{\text{minima}} E_{\text{minima}}(s_C(u)) + \\ & k_{\text{edge}}(E_{\text{edge}}(s_L(u)) + E_{\text{edge}}(s_R(u))) \end{aligned}$$

The center of the combination snake seeks minima and is intended to find the center of an artery, where the image is most opaque. The offset parts of the combination snake seek edges. The combination of the two energies is more effective than the individual energies alone.

There are several free parameters to set.

- k_{minima}, the strength of the minima-seeking energy
- k_{edge}, the strength of the edge-seeking energy
- r_{width}, radius to seek

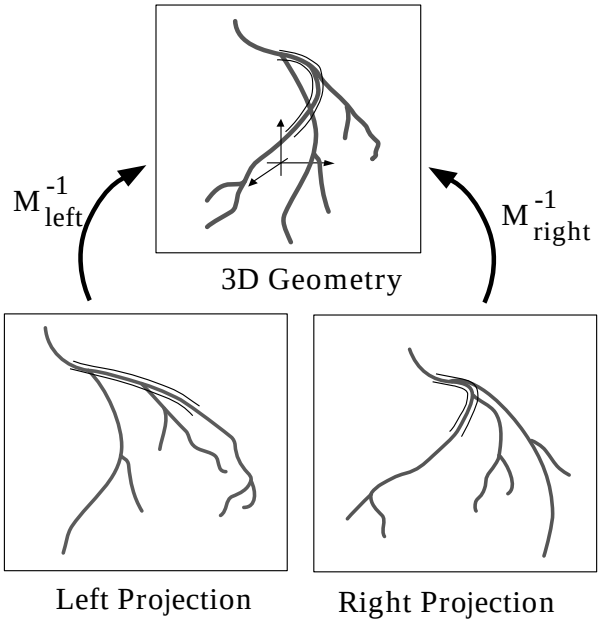

Figure 4: Stereo Matching

For the work described here, the constants were set with initial rough estimates and then tuned interactively for good performance. Ideally, these parameters should be assigned from measurements of the physical properties of the actual catheter and actual vessels. This might eliminate the need for a tuning step.

Note that for this particular formulation, r_{width} is an input parameter specifying the desired size of the matching artery. To make the combination snake more general, the radius could be made a function of u.

2.2 Stereo Matching

We require at least two views to reconstruct the centerlines of the arteries (Figures 3 and 4). We use two of the compound snakes as described above, with an additional energy that tries to minimize the distance between the two snakes in three-dimensions:[3]

$$E_{\text{stereo}}(u) = |M^{-1}_{left}(S_{0_{left}}(u)) - M^{-1}_{right}(S_{0_{right}}(u))|^2$$

where M^{-1} is the inverse of the projection transformation and the subscripts $left$ and $right$ refer to the two projected views. M^{-1} is usually taken as a 4×4 perspective matrix, but the snake energy based method can also include nonlinear warping corrections for distorted camera images. Although we have not yet incorporated this, the warping function can be calculated by imaging a regular grid and calculating the inverse warping function.

2.3 Snakes in 3D

Since we are reconstructing a three-dimensional geometric structure, it makes sense to use a three-dimensional model. The technique we use is similar to the two-dimensional energy functionals described previously, but we use one snake in three dimensions and project to two dimensions to express the energy functionals (Figure 2.3) This is similar to other work by the original snake authors[12].

We use the two two-dimensional snakes as above to get an initial position for the three-dimensional snake. Once we have a single snake, we no longer have the parametrization problems that occur when using two different snakes.

As described in the original paper by Kass [3], the internal energy is given by

$$E_{\text{internal}} = (\alpha(s)|v_s(s)|^2 + \beta(s)|v_{ss}(s)|^2)/2$$

which works in two and three dimensions, but with a slightly different interpretation of the terms (there is no torsion in two dimensions).

Let $s_C(u)$ be the centerline of the snake in three dimensions. We will define $s^0_C(u)$ and $s^1_C(u)$ to be $s_C(u)$ transformed by the projections M^{left} and M^{right}, respectively.

$$\begin{aligned} s^0_C(u) &= M^{left} s_C(u) \\ s^1_C(u) &= M^{right} s_C(u) \end{aligned}$$

Then as above we define s^i_L and s^i_R to be perpendicularly offset from $s^i_C(u)$ at each u by r_{width}. Let

$$\begin{aligned} s^i_L(u) &= s^i_C(u) + r_{\text{width}} n^i(u) \\ s^i_R(u) &= s^i_C(u) - r_{\text{width}} n^i(u) \end{aligned}$$

where $n^i(u)$ is the normal to the curve of $s^i_C(u)$ in the projected plane. Since s^i_C is a projection, it is possible that non-zero segments of the original curve s_C will project onto a single point. For such cases, n^i will have degeneracies. To handle these degenerate cases and to prevent sudden sign flips, the discretized version of n^i is constrained to be positive and on just one side of s^i_C. This is accomplished by sequentially testing the dot product of the candidate normal with the previous discretized point's normal. If the dot product is close to or equal to zero, the previous point's normal is used. If less than zero, then the new normal is flipped.

Once we have the two offset curves and centerlines in both projections, we use the same formulation for the energies as in the previous section—the centerline seek minima and the offset curves seek edges.

The energy equation is solved by taking a variational derivative which gives rise to a set of Euler equations. The solution technique as described in [3] requires the partial derivatives of the external energy function. Since the snake is now 3D, we need derivatives in the x, y, and z coordinates of the artery.

But the energy terms are described in the coordinates of the plane of the projections. Thus, we must multiply the vector of partial derivatives by the inverse jacobian matrix of the transformation. If we consider the two projection transformations as 4×4 matrices, then the inverse jacobian matrices are just the inverses of the matrices. If we include the de-warping grid, then we also need a local inverse jacobian of the de-warping function.

Once we have the partial derivatives f_x, f_y, and f_z in the artery coordinates, we can use the same solution technique as for the two-dimensional snakes, using the LU-decomposition inverse of a pentadiagonal banded matrix that handles the implicit step for the internal energy and an explicit Euler step for the external energy.

Figure 5 shows the two-dimensional snakes in each of the angiograms tracking the same section of artery and the reconstructed result. The three-dimensional display of the angiograms along with the computed three-dimensional artery centerline clearly shows the geometric relation of the two projections with the result.

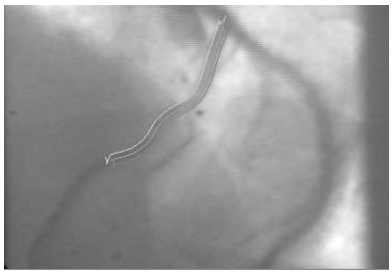

(a) Left Snake

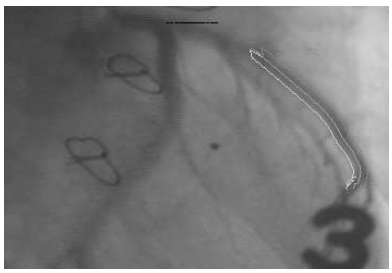

(b) Right Snake

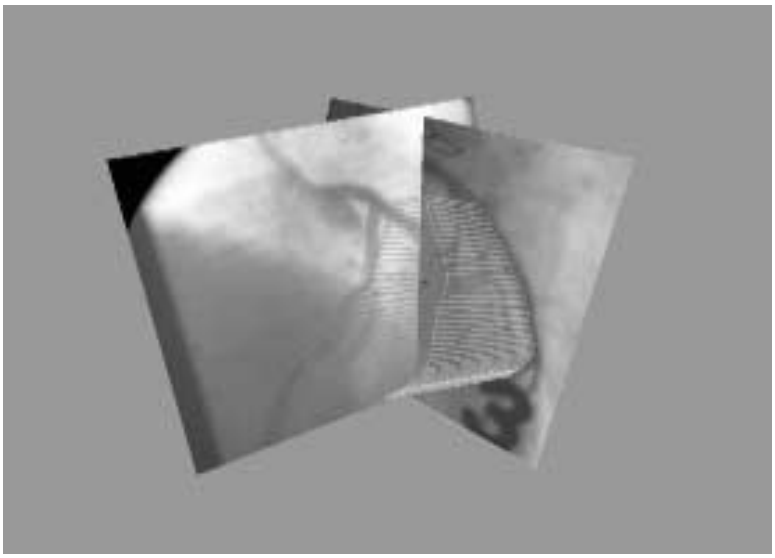

(c) Computed 3D artery centerline.

Figure 5: Left and right projections with snakes and the resulting 3D snake

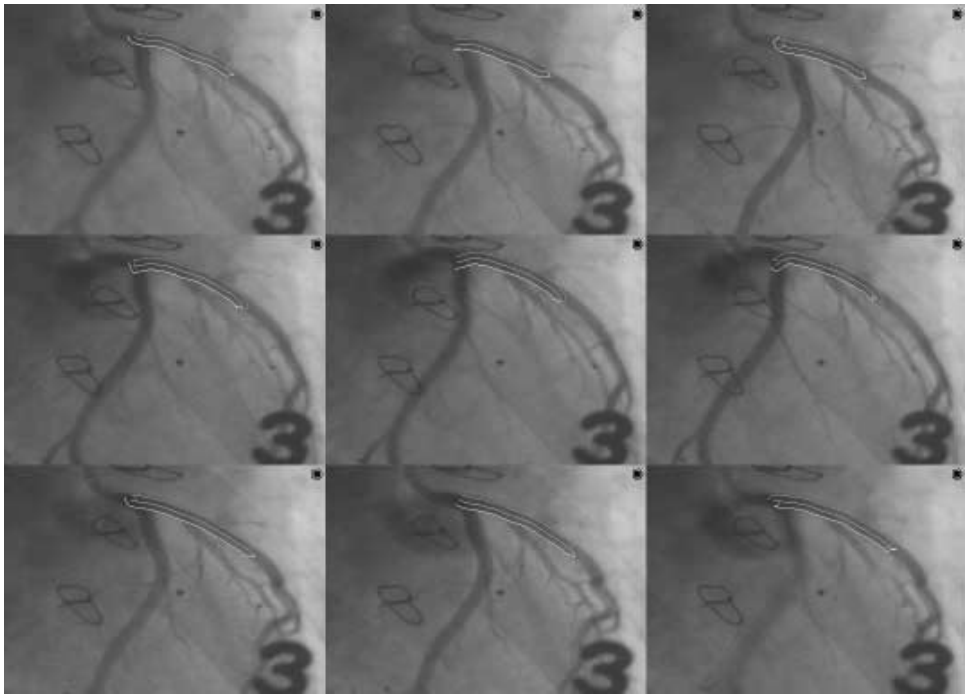

Figure 6: Motion Tracking — Sequence of frames showing inter-frame tracking of arteries by composite snake.

3 Motion Tracking

The computation for the snakes involves a simulated elastic system that is evolved forward in time. Since time is built into the calculation, it is straightforward to let the images change with time. The snakes will track the local minima (Figure 6) as long as the jumps in the motion between successive frames are not too large.[3] We worked with angiogram data sets from heart-transplant patients whose heart rates were elevated up to 120 beats per minute. This made the jumps between frames more pronounced, and our snakes tended to jump out of the proper local minima. Since arteries have mass and a smoothly changing velocity, we added a mass term to the snake which helped to predict where the artery would be.[3][1] This mass term is calculated by keeping track of the previous two time steps for the snake and estimating acceleration. The mass term only became effective when the weighting term and the number of relaxation steps were tuned.

Since the snakes seek local minima in the energy functions, it is important to start them with the proper initial conditions, or they will find the wrong local minima. For the first frame, we set the initial position of the snake in both of the stereo images by interactively sketching a series of line segments over the desired artery segment. The snake was then activated and allowed to relax into the local minimum in each frame. Then the stereo energy weight was ramped from 0 to 1, allowing the two snakes to find a good stereo match. The above steps were all done on a single stereo-pair angiogram. The rest of the motion was tracked automatically, using the previous frames to estimate the starting location of subsequent frames. Certain highly curved sections of the artery needed interactive adjustment to make the snake track properly.

4 Positioning of Time-Dependent 2D Ultrasound Slices

Landmark sites, located at branching points in the ultrasound sequence, are used to orient the slices (Figure 7). Each landmark shows a correspondence between a sidebranching vessel in the ultrasound data and in the angiographic data. These sidebranches are used to orient the slice data around the centerline of the artery. The current arclength of the catheter, as measured relative to a landmark site (or by a linear encoder on the shaft), is used to get the slice's distal location along the arterial tree. The distal location maps directly to a 3D location, since we have already calculated the 3D geometry of the arterial tree and catheter path.

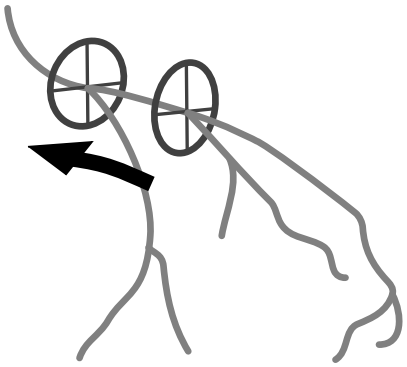

Figure 7: Landmark Sites

This calculation is complicated by the time-dependence of both the arterial tree and the catheter arclength as it is pulled back. Assume that the arterial tree motion is cyclic (regular heartbeat) and that either the catheter arclength versus time is linear or measurable with a linear encoder. Also assume that the distortion of the vessel due to the catheter is negligible. Then for a given time, we know both the phase of the arterial tree (point in the cardiac cycle) and the distal location and thus the geometric position of the ultrasound slice relative to the current arterial tree geometry. Future testing with physical phantoms will be needed to get error bounds on these assumptions.

Figure 8 plots the spacetime path of one coordinate (x, y, or z) of the moving arterial tree and shows the path of the transducer moving in the surface that results. The difficulty is that sequential slices represent not only different positions along the artery centerline, but are taken at different phases of the cardiac cycle. The slices active at a given cycle phase are the slices from transducer distal locations whose times modulo the cycle period T correspond to the same phase. Thus slices $t_0, t_0 + T, t_0 + 2T, \ldots$ are all active slices of the same cycle. Thus the problem is reduced to one of retrieving the appropriate ultrasound slice for each specific space-time position.

To dynamically display the cross-sectional images, the complete set of ultrasound slices must be assembled for each phase of the cardiac cycle.

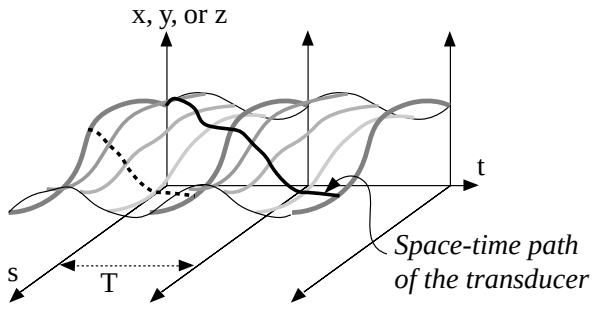

Figure 8: Path of transducer relative to heart cycle. The slices are reorganized so that for each frame the only slices shown are those that match the artery centerline's phase of the heart cycle.

5 Examples

Figure 9(a) shows a static image of the ultrasound slices placed along the artery centerline, with a sagittal split applied to each slice to reveal the internal structure of the arterial wall. Figure 9(b) shows a coronal split applied to each slice.

The dark semi-circle in the very center of each ultrasound frame is the ring-down region in which no data is received. The larger dark circular region is the lumen of the vessel through which the blood flows. The white region beyond the lumen in each of the slices shows the interior structure of the vessel wall. Since the x-ray contrast dye flows in the blood, the lumen is all that appears in the two projected angiograms. Note how the positioning of the slices with the reference of the two projected angiograms clearly shows the relation of the slices to the curved geometry of the artery.

6 Volume Rendering

Originally we attempted to use a parametric interpolation volume imaging technique to portray the three-dimensional information.[5] Unfortunately, with the pullback rates used, the sample spacing between slices was an order of magnitude larger than the in-slice resolution, yielding interpolated volumes which were too smooth to be useful for diagnosis (Figure 10). We are currently try to obtain images at slower pullback rates providing more closely packed slices.

Another drawback to volume rendering is the long time typically needed to render a frame (approximately one hour with the current testbed.)

7 Conclusion

By recovering the moving three-dimensional arterial tree and placing the slices at their proper positions in time and space, we are able to combine the strengths of both intravascular ultrasound and x-ray angiograms. For the first time, the moving geometry of the artery from the angiogram and the time-dependent images of the interior of the vessel wall from the intravascular ultrasound can be viewed simultaneously, with proper geometric relations.

There are several limitations to the technique described here which should be the subject for future work. First, the use of the centerline of the artery to place the slices is an approximation, since the catheter is, in general, off-center and tilted with respect to the artery. This may be corrected by recovering the path of the catheter and transducer relative to the artery centerline — we are pursuing a technique that uses the offset and elliptical shape of the lumen in the ultrasound slices.

Second, the correlation of ultrasound slice and angiogram timing is inexact, but this is easily corrected by using digital data marked with the current heart cycle from an electrocardiogram.

Third, there is a substantial tuning step required to find the proper parameters for the artery-seeking snakes. One possible approach to avoid this tuning step would be to use a three-dimensional snake with the internal elastic energy constants corresponding to the measured elastic properties of actual arteries and catheters. The image-seeking energy weights could then be set relative to the resulting physically-based snake.

Other future work includes using a slow pullback to obtain a dataset with more closely spaced slice data, and applying the techniques described here to experimentally reconstruct, render, and compare a physical phantom with known geometry.

Ultimately, with greatly increased machine speed and closely spaced slice data, volume rendering the dynamic data may prove to be more effective than showing just the slice data, particularly for views that are nearly parallel to a slice.

By using texture-mapped rectangles the combined ultrasound slice/angiogram display technique is well suited to run in real time on current graphics workstations. Accurate knowledge of the dynamic interior anatomy of the diseased vessel will permit improved diagnostic techniques for the physician attempting angioplasty or atherectomy. We hope that this kind of display will move into the interventional catheter laboratory.

Acknowledgements

Thanks to Jon Blocksom without whom the paper would not have been completed. Thanks to Peter Shirley and Dan Kartch for help with the document preparation, to Alan Yeung, Edwin Alderman, and Peter Fitzgerald for providing datasets and insight. Thanks to Allison Hart. This work was supported by the NSF/ARPA Science and Technology Center for Computer Graphics and Scientific Visualization (ASC-8920219) and performed on workstations generously provided by the Hewlett-Packard Corporation.

References

[1] Hyche, M., Ezquerra, N., and Mullick, R. Spatiotemporal detection of arterial structure using active contours. *Proceedings of Visualization in Biomedical Computing 1808* (1992), 52–62.

[2] Isner, J. M., Rosenfield, K., Losordo, D. W., and Krishnaswamy, C. Clinical experience with intravascular ultrasound as an adjunct to percutaneous revascularization. In Tobis and Yock [13], part 16, pp. 186–197.

[3] Kass, M., Witkin, A., and Terzopoulos, D. Snakes: Active contour models. *International Journal of Computer Vision* (1988), 321–331.

[4] Krishnaswamy, C., D'Adamo, A. J., and Sehgal, C. M. Three-dimensional reconstruction of intravascular ultrasound images. In Tobis and Yock [13], part 13, pp. 141–147.

[5] Lengyel, J., Greenberg, D. P., Yeung, A., Alderman, E., and Popp, R. Three-dimensional reconstruction and volume rendering of intravascular ultrasound slices imaged on a curved arterial path. In *Proceedings of CVRMed'95* (Apr. 1995).

[6] MacKay, S. A., Sayre, R. E., and Potel, M. J. 3d galatea: Entry of three-dimensional moving points from multiple perspective views. *Proceedings of SIGGRAPH'82 (Boston, Massachusetts, July 26–30, 1982) 16*, 3 (July 1982), 213–222.

[7] Roelandt, J. R., di Mario, C., Pandian, N. G., Wenguang, L., Keane, D., Slager, C. J., de Feyter, P. J., and Serruys, P. W. Three-dimensional reconstruction of intracoronary ultrasound images. *Circulation 90* (1994), 1044–1055.

[8] Rosenfield, K., Losordo, D. W., Ramaswamy, K., Pastore, J. O., Langevin, E., Razvi, S., Kosowsky, B. D., and Isner, J. M. Three-dimensional reconstruction of human coronary and peripheral arteries from images recorded during two-dimensional intravascular ultrasound examination. *Circulation 84* (1991), 1938–1956.

[9] St. Goar, F., Pinto, F. J., Alderman, E. L., Fitzgerald, P. J., Stadius, M. L., and Popp, R. L. Intravascular ultrasound imaging of angiographically normal coronary arteries: An in vivo comparison with quantitative angiography. *Journal of the American College of Cardiology 18* (1991), 952–958.

[10] St. Goar, F., Pinto, F. J., Alderman, E. L., Valantine, H. A., Schroeder, J. S., Gao, S.-Z., Stinson, E. B., and Popp, R. L. Intracoronary ultrasound in cardiac transplant recipients—in vivo evidence of "angiographically silent" intimal thickening. *Circulation 85* (1992), 979–987.

[11] Terzopoulos, D., Witkin, A., and Kass, M. Symmetry-seeking models and 3d object reconstruction. *International Journal of Computer Vision 1* (1987), 211–221.

[12] Terzopoulos, D., Witkin, A., and Kass, M. Contraints on deformable models : Recovering 3d shape and nonrigid motion. *Artificial Intelligence 35* (1988), 91–123.

[13] Tobis, J. M., and Yock, P. G., Eds. *Intravascular Ultrasound Imaging.* Churchill Livingstone Inc., New York, 1992.

[14] Yock, P., Johnson, E., and David, D. Intravascular ultrasound: Development and clinical potential. *American Journal of Cardiac Imaging 2* (1988), 185–193.

[15] Yock, P., Linker, D., and Angelson, A. Two-dimensional intravascular ultrasound: Technical development and initial clinical experience. *Journal of the American Society of Echocardiography 2* (1989), 296–304.

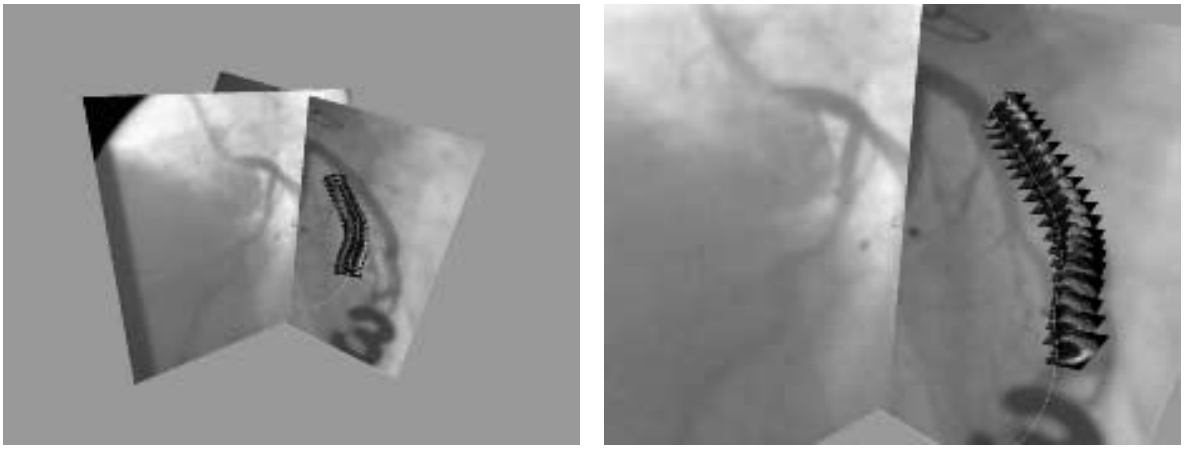

(a) Coronal Split (b) Sagittal Split

Figure 9: Slices Positioned Along the Transducer Path

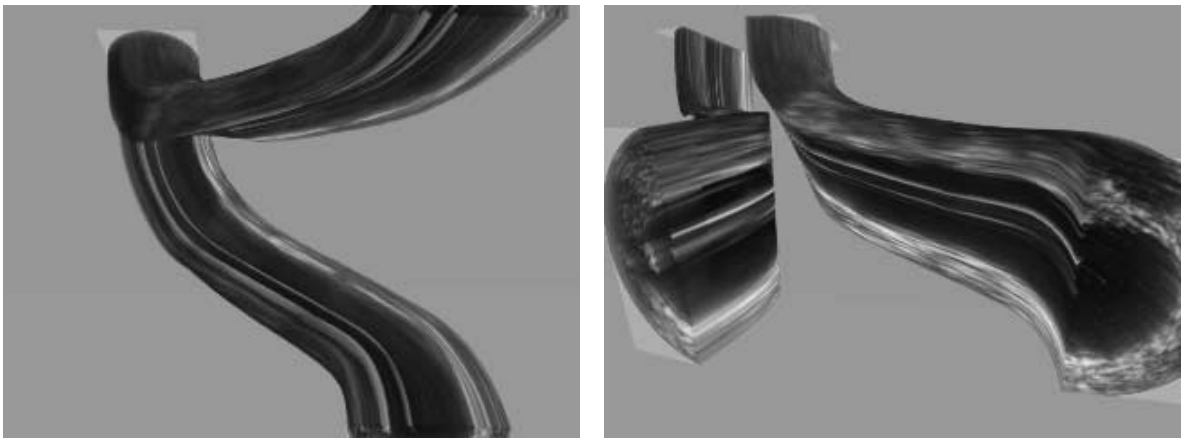

(a) Coronal Split (b) Sagittal Split

Figure 10: Volume-Rendered Images